Synthetic and Systems Biotechnology 13 (2026) 531–544

Contents lists available at ScienceDirect

Synthetic and Systems Biotechnology

journal homepage: www.keaipublishing.com/en/journals/synthetic-and-systems-biotechnology

Original Research Article

S267P mutation of OxyR regulator in *Zymomonas mobilis*: mechanism of oxidative stress tolerance and applications in cellulosic hydrolysate fermentation and oxidative stress monitoring

Yi Wang [a,1], Binan Geng [a,*,1], Shuyi Liu [a], Yalun Wu [a], Shihui Yang [a,b,**]

[a] School of Life Sciences, Hubei University, Wuhan, 430062, China
[b] Wuhan ZymoBiotech Inc, Wuhan, 430077, China

ARTICLE INFO

Keywords:
OxyR
Oxidative stress
Inhibitor tolerance
Transcriptomics
Biosensor
Zymomonas mobilis

ABSTRACT

The peroxide-sensing transcriptional regulator OxyR plays a pivotal role in bacterial oxidative stress responses. The OxyR^{S267P} mutation was previously identified in *Zymomonas mobilis* ZMNP, a mutant strain with enhanced hydrolysate tolerance. To investigate the biological function of revert strain and the corresponding mutant, phenotypic, transcriptomic, structural, and functional analyses were performed. The fermentation performance of strain ZMNPC in toxic xylose mother liquor had similar slow substrate utilization profile as that of the wild-type strain ZM4 with an approximate 20 h lag behind strain ZMNP. Transcriptomic analysis revealed constitutive downregulation of genes involved in reactive oxygen species (ROS) detoxification, cysteine biosynthesis, redox homeostasis, and macromolecular repair in strain ZMNPC, which is consistent with higher intracellular ROS levels and reduced survival under H_2O_2. Protein structural modeling demonstrated that S267P relieves steric hindrance near disulfide bond-forming cysteines, promoting OxyR activation, molecular dynamics simulations indicated that the OxyR mutation stabilizes the oxidized conformation, binding reactions showing enhanced DNA-binding affinity of OxyR^{S267P}, and gene expression results confirmed OxyR^{S267P} upregulates ROS clearance genes under different inhibitor stress conditions. We further developed oxidative-stress biosensors OxyR^{S267P}–P1732 and OxyR^{S267P}–P1753 based on this regulatory module. Our study confirms OxyR^{S267P} as a key determinant of robust oxidative stress tolerance in *Z. mobilis*, providing mechanistic insights to guide the development of novel regulatory tools for biosensing and metabolic engineering.

1. Introduction

Molecular oxygen and environmental factors such as ozone exposure, hyperoxia, ionizing radiation, and heavy metal ions can lead to the accumulation of intracellular reactive oxygen species (ROS), which can damage cellular macromolecules such as DNA, proteins, carbohydrates, and lipids as well as cell processes such as chromosome deletions, single strand breaks, DNA mutations, DNA-protein crosslinks, lipid peroxidation, and membrane damage [1–6]. Therefore, the timely clearance of intracellular ROS is crucial for industrial microorganisms to achieve a robust growth and high-yield production. Living organisms have evolved diverse antioxidant systems to protect themselves against the harmful effects of ROS, which include global regulators such as OxyR, SoxRS, PerR, and OhrR that are usually regulate genes associated with enzymes capable of reducing ROS or repairing oxidative damage to prevent, counteract, and repair damages caused by ROS [7].

OxyR, a 34 kDa protein that forms a homotetramer, is a widely conserved peroxide-sensing LysR family transcriptional regulator in bacteria [8]. The OxyR regulator was first discovered in *Salmonella typhimurium*, and has also been identified in more than 20 bacteria such as *Escherichia coli* and *Pseudomonas aeruginosa* [1,9–12]. OxyR consists of an N-terminal DNA-binding domain (DBD) and a C-terminal

Peer review under the responsibility of Editorial Board of Synthetic and Systems Biotechnology.
* Corresponding author.
** Corresponding author. School of Life Sciences, Hubei University, Wuhan, 430062, China.
E-mail addresses: ee.wang@stu.hubu.edu.cn (Y. Wang), binangeng@hubu.edu.cn (B. Geng), shuyiliu@stu.hubu.edu.cn (S. Liu), aaronwu@stu.hubu.edu.cn (Y. Wu), Shihui.Yang@hubu.edu.cn (S. Yang).
[1] These authors contributed equally to this work.

https://doi.org/10.1016/j.synbio.2026.03.010
Received 10 February 2026; Received in revised form 1 March 2026; Accepted 15 March 2026

regulatory domain (RD) [13]. The three-dimensional crystal structure of the reduced and oxidized OxyR protein revealed Cys_{199} and Cys_{208} as conserved sites in *E. coli*, and the oxidation of the two cysteine residues on the OxyR protein plays an essential role in its redox-sensing mechanism [14–17]. The conserved Cys_{199} (Cys_{199}-SOH) is rapid S-hydroxylation in the presence of H_2O_2, followed by the rapid formation of an intramolecular disulfide bond with the second conserved Cys_{208} that allow the protein to bind to its target promoter region for transcriptional activation [18]. OxyR regulates about 40 genes including *ahpC*, *grx*, *gor*, *trxC*, *katA*, *dps*, *ftn*, *cydA*, *fur*, and *sufABCDSE* operon that help protect cells from oxidative stress [19,20]. Point mutations in *oxyR*, acquired through adaptive evolution to acidic-pH, lactate, or iron supplementation, lead to increased expression levels of OxyR-regulated genes [21,22]. This demonstrates that OxyR is crucial for bacterial adaptation to inhibitory environments.

Zymomonas mobilis is an ideal industrial microbial chassis for lignocellulosic bioproducts due to its remarkable capacity for converting biomass into biochemicals [23,24]. *Z. mobilis* possesses a suite of advantageous traits including tolerance to inhibitors [25], resistance to acids [26] and high temperatures [27], and rapid sugar utilization via its unique anaerobic Entner-Doudoroff pathway [23]. The establishment of advanced gene-editing tools has further enabled the construction of *Z. mobilis* recombinant strains for biochemical production [24,28–37]. However, lignocellulosic hydrolysates contain inhibitory compounds like acetate and furfural triggering the formation of ROS [25]. Consequently, this oxidative stress impairs the growth and metabolism of *Z. mobilis*, leading to reduced product yields and prolonged fermentation cycles.

Genes involved in ROS detoxification and cell damage repair in *Z. mobilis* were upregulated under different stress conditions, including high temperature, acidic-pH and furfural supplementation [13,25,38–41]. A specific T7K mutation within the N-terminal of helix–turn–helix (HTH) DNA-binding domain of OxyR was previously reported to enhance the expression of ROS detoxification genes, such as *ZMO0918* encoding catalase and *ZMO1060* encoding superoxide dismutase, in acidic-pH tolerant mutant strains *Z. mobilis* 3.5 M and 3.6 M [13]. In addition, a S267P mutation was identified in the global regulator OxyR of strain ZMNP, a plasmid-free derivative of strain ZM4, which may be related to the significant decrease of intracellular ROS levels and the consequent improved fermentation performance in a toxic xylose mother liquor [42]. Multi-omics studies also indicated that the expression of multiple antioxidant-related genes was upregulated in strain ZMNP. Collectively, these findings indicate that the $OxyR^{S267P}$ mutation may modulate the expression of downstream antioxidant genes [42], and thereby strengthen cellular oxidative stress tolerance and robust fermentative production.

Since oxidative stress severely inhibited the physiology and growth of microorganisms, which is induced from conditions that are constantly encountered by microorganisms such as pH, temperature, toxic end-products such as alcohols and organic acids, and inhibitory chemicals within lignocellulosic hydrolysates such as furfural, hydroxymethylfurfural (HMF), and phenolic compounds, the investigation of key molecular determinators and underlying mechanisms associated with oxidative stress responses could help improve microbial robustness. This study thus aimed to investigate the correlations between $OxyR^{S267P}$ mutation and the enhanced oxidative stress tolerance in strain ZMNP and elucidate the molecular mechanisms underlying this mutation-mediated intracellular ROS tolerance in *Z. mobilis*, which will provide genetic targets to enhance strain robustness and improve fermentation performance in inhibitory conditions such as lignocellulosic hydrolysates.

2. Materials and methods

2.1. Strains, media, and culture conditions

E. coli DH5α was cultured in Luria-Bertani (LB) medium (10 g/L NaCl, 10 g/L tryptone, 5 g/L yeast extract) at 37 °C with shaking speed at 220 rpm. *Z. mobilis* ZM4, ZMNP, and ZMNPC were cultured in rich medium (RM, 50 g/L glucose, 10 g/L yeast extract, 2 g/L KH_2PO_4) at 30 °C. When required, 100 μg/mL spectinomycin was used for both *E. coli* and *Z. mobilis*, 50 μg/mL chloramphenicol was used for *E. coli* and 100 μg/mL chloramphenicol was used for *Z. mobilis*. The final concentrations of furfural, ethanol, or acetate added to RM medium were 2.60 g/L (RMF), 47.36 g/L (RME), and 12 g/L (RMA), respectively. The xylose mother liquor used in this study was provided by Zhejiang Huakang Pharmaceutical Co., Ltd (Kaihua, Zhejiang, China). The hydrolysate stock solution contained 216.87 g/L glucose, 103.98 g/L xylose, 4.44 g/L furfural, and 1.18 g/L acetate. The hydrolysate was diluted with 10 × RM^- medium (100 g/L yeast extract, 20 g/L KH_2PO_4) for fermentation. *E. coli*, *Z. mobilis*, and their derivative strains used in this study are listed in Table S1.

2.2. Construction of editing plasmid and candidate promoter plasmids

The editing plasmid for $OxyR^{S267P}$ mutation reversion was constructed based on native Type I–F CRISPR-Cas system as previously described [43]. The gRNA sequence was annealed using two single-stranded oligonucleotides of oxyR-gR-F and oxyR-gR-R, and then ligated into *Bsa*I (NEB, USA) linearized pL2R by T4 ligase (TaKaRa, Japan). The oligonucleotide primer pairs oxyR-US-F and oxyR-US-R were used to amplify the upstream flank sequence of *oxyR*, and oxyR-DS-F and oxyR-DS-R were used to amplify the downstream flank sequence using Primer STAR polymerase (TaKaRa, Japan). The pL2R vector containing the gRNA was amplified using primers pL2R-FK-F and pL2R-FK-R.

The IDRS (Insulated Dual Reporter System) [44] was used to quantify the candidate promoters of genes exhibiting significant differential expression under OxyR regulation. The IDRS system expresses *opmCherry* as an internal reference, while the promoter of *eGFP* is replaced with the test promoter. The vector of pIDRS was amplified using primers V-pIDRS-F and V-pIDRS-R. The candidate promoters were amplified using strain ZM4 genomic DNA. The resulting PCR product was then assembled by T5 Exonuclease Kit (NEB, USA) and recombinant constructs were then selected on LB agar plates supplemented with antibiotics of spectinomycin or chloramphenicol. Subsequently, transformants containing the correct plasmid constructs were verified by colony PCR and Sanger sequencing (TsingKe, Wuhan, China). The plasmids and primers used in this study are listed in Table S2 and Table S3.

2.3. Electroporation transformation and strain selection

Plasmids were extracted and quantified using a NanoDrop spectrophotometer (NanoDrop Technologies, USA), and electroporation was performed using 0.5–2 μg of plasmids with the Gene Pulser system (Bio-Rad, USA) with the settings of 1.6 kV/cm, 25 μF, and 200 Ω. Immediately following the electroporation, 1 mL of pre-warmed RM recovery medium was added to the cuvette. The cell suspension was then transferred to a sterile tube and incubated at 30 °C for 4~6 h to allow for phenotypic expression. Finally, the cells were spread onto RM agar plates containing spectinomycin or chloramphenicol and incubated until colonies appeared.

2.4. Flask fermentation and analytic methods

Z. mobilis strains ZM4, ZMNP, and ZMNPC were prepared by inoculating glycerol stocks first into 1 mL of RM medium. After static incubation at 30 °C, the cultures were transferred to 50 mL tubes containing

40 mL of RM medium and grown statically at 30 °C to mid-logarithmic phase. These seed cultures were then used to inoculate 250 mL flasks containing 200 mL of RM medium, which were incubated at 30 °C until they reached mid-log phase. For the fermentation experiments, the secondary cultures were inoculated into 50 mL shake flasks containing 40 mL of RM, RMA, RMF, or RME medium and 1/3 of the secondary master mix, to an initial $OD_{600\ nm}$ of 0.1. Cultures were incubated at 30 °C with shaking speed at 100 rpm. No active aeration, sparging, or dissolved oxygen control was applied. Bacterial growth was monitored by measuring the maximum biomass at various time points using a UV-1800 spectrophotometer (AOELAB, China).

During the shake-flask fermentation, samples were collected at designated time points for metabolite concentration quantification. Each 1 mL sample was centrifuged at 12,000 rpm for 1 min, and the resulting supernatant was filtered through a 0.22 μm membrane. The concentrations of glucose and ethanol in the filtrate were quantified by high-performance liquid chromatography (HPLC). The HPLC system (Shimadzu, Japan) was equipped with an Aminex HPX-87H column (Bio-Rad, USA) and a refractive index detector. The analysis was performed at 60 °C using 5 mM H_2SO_4 as the mobile phase, with a flow rate of 0.5 mL/min. All experiments were performed with at least three independent biological replicates.

2.5. RNA-seq transcriptomic analysis

Transcriptomic analysis was performed as previously described [42]. Briefly, *Z. mobilis* strains ZMNPC and ZMNP were cultured in RM medium, and cells were harvested at the mid-log phase for RNA extraction. Subsequent RNA sequencing was conducted by GENEWIZ Bio Inc. (Suzhou, China) on an Illumina HiSeq 2000 platform.

The raw sequencing data in fastQ format were subjected to quality assessment using FastQC (Babraham Bioinformatics, UK). Based on the quality reports, adapter sequences and low-quality bases were trimmed to ensure data reliability. Read mapping and expression quantification were performed using the CLC Genomics Workbench (version 14.0, Invitrogen, USA), with the ZMNP genome sequence serving as the reference. Gene expression levels were estimated and normalized using the RPKM metric.

For differential expression analysis, the RPKM values were further processed and statistically evaluated with R software (Rversion 4.5.3, Vienna, Austria). DESeq2 was applied, which models RNA-seq count data based on a negative binomial distribution. Genes with a adjust *p*-value <0.05 and an absolute $\log_2$-fold change ≥ 1 were defined as significantly differentially expressed.

2.6. Measurement of intracellular ROS

Intracellular ROS levels were assessed using the fluorescent probe H_2DCF-DA (Baitai Biotechnology, China). One $OD_{600\ nm}$ Cells were harvested at the logarithmic growth phase, washed once with phosphate-buffered saline (PBS), and then resuspended in 500 μL of 1 × PBS. The cell suspension was loaded with 100 μM H_2DCF-DA and incubated in the dark at 30 °C, 100 rpm for 1 h. Following incubation, the cells were washed three times with 1 × PBS and finally resuspended in 300 μL of 1 × PBS for analysis. Fluorescence intensity was measured using a CytoFLEX flow cytometer (Beckman Coulter, USA) with an excitation wavelength of 488 nm and an emission wavelength of 525 nm. For each sample, 20,000 cellular events were collected, and cells with fluorescence intensity between 10^3 and 10^5 were gated for subsequent statistical analysis. All experiments were performed with at least three independent biological replicates.

2.7. Measurement of survival rate after H_2O_2 shock

Overnight cultures of ZM4, ZMNP, and ZMNPC strains were inoculated into fresh RM medium at an initial $OD_{600\ nm}$ of 0.1 and grown to the mid-logarithmic phase. The bacterial cultures were subjected to oxidative stress by adding 30% (v/v) H_2O_2 to achieve final concentrations of 0.5 mM and 1 mM, respectively. After thorough mixing, the treated cultures were incubated at 30 °C for 10 min. Control groups without H_2O_2 supplementation were processed simultaneously under identical conditions. Following the treatment, all samples were serially diluted with RM medium, spread evenly onto RM agar plates, and incubated at 30 °C for 2 days. The survival rate was calculated by enumerating the colony-forming units (CFU) after treatment and comparing them to the untreated control. All experiments were performed with at least three independent biological replicates.

2.8. Heavy ion beam mutagenesis and ARTP mutagenesis and fatality rate detected

For heavy ion beam mutagenesis, the first step was the preparation of cell cultures. Strains of *Z. mobilis* ZM4 and ZMNP recovered from glycerol stock solution were inoculated into 5 mL RM medium at 30 °C. The overnight culture was then transferred into 50 mL shake flasks with 40 mL medium at an initial $OD_{600\ nm}$ of 0.05, and cultured at 30 °C, 100 rpm. Cell cultures were harvested in logarithmic phase, washed once with sterilized 30% glycerol. Cell pellet was then resuspended with sterile 30% glycerol to an $OD_{600\ nm}$ value of 0.8. Finally, 1 mL cell suspension was taken into a sterile dish. The second step was irradiation mutagenesis. The $^{12}C^{6+}$ ions were accelerated up to 80 MeV/μ by the Heavy Ion Research Facility (HIRFL, China) at Institute of Modern Physics, Chinese Academy of Sciences (IMP-CAS). By using an absorber with a specific thickness, the average LET value was calculated to be 31 keV/μm. The cell suspension in a sterilized dish was irradiated at gradient doses of 40, 120, and 200 Gy, respectively, which were then spread on the RM plate after dilution.

For ARTP mutagenesis, the first step was same as heavy ion beam mutagenesis. The second step was mutagenesis. Seed culture was washed with sterilized 0.85% NaCl, and cell pellet was then resuspended with sterilized 2% glycerol to an $OD_{600\ nm}$ value of 0.6∼0.8. Finally, 10 μL suspension was evenly spread on the sterilized metal plate and then treated with pure helium plasma under 120 W radio-frequency power input and 10 SLM helium flow rate using an ARTP Breeding Mutagenesis Machine (ARTP-M model, Yuanqing Tianmu Biotechnology Co., Ltd., China). The metal plate was immediately placed into a sterilized tube containing 1 mL sterile 0.85% NaCl after mutagenesis. An appropriate dilution of the resulting cell suspension was spread on RM plates and cultivated at 30 °C for 48 h. All experiments were performed with at least three independent biological replicates.

The colonies were counted manually and the fatality rate of the heavy ion beam mutagenesis and ARTP treatment was calculated using the following equation:

Fatality rate $= (1 - C_i/C_c) \times 100\%$;

where C_i is the colony number counted on plates after irradiation; C_c is the colony number counted on plates without irradiation.

2.9. In silico analysis of the OxyR mutant

The amino acid sequences of OxyR from 17 experimentally characterized bacterial strains from the UniProt database were downloaded, which were compared with the wild-type and OxyR mutant in *Z. mobilis* ZM4 for OxyR conservation and divergence using multiple sequence alignment based on MEGA with sequence similarity setting greater than 70%. The atomic coordinate files (PDB: 1I69 and 1I6A) was used to determine the amino acid distances between the mutation and the previously published mutations with known OxyR activity [21] by PyMOL 3.1 and BIOVIA Discovery Studio 2021. The heatmap for visualization was generated using the *Seaborn* python package.

The online structure prediction service provided by the Protenix website (https://protenix-server.com) was employed to predict the tetrameric complex structures of *Zymomonas mobilis* wild-type OxyR and

the OxyR^{S267P} mutant, both in the presence and absence of H_2O_2 binding. After obtaining the initial complex structures, structural repair and preprocessing were performed using YASARA software (Version 20.10.4), followed by molecular dynamics (MD) simulations. The MD simulation system was solvated in a 0.9% sodium chloride (NaCl) solution, with the temperature set to 30 °C and pH to 7.5. Periodic boundary conditions were applied to construct the solvated system, and the total duration of the simulations was 40 ns. All other simulation parameters were set in accordance with those reported previously [18].

2.10. Electrophoretic mobility shift assays (EMSAs)

Electrophoretic mobility shift assays (EMSAs) were performed to compare the DNA-binding affinities of wild-type OxyR and OxyR^{S267P} mutant. For initial optimization and rapid screening of protein concentration ranges, EMSAs were first conducted using native agarose gels, which allowed efficient and rapid visualization of protein-DNA complex formation with relatively long DNA probes. Prior to binding reactions, purified OxyR proteins were oxidized by incubation with 100 μM H_2O_2 for 5 min at room temperature. Excess H_2O_2 was immediately removed by rapid desalting to prevent further oxidation. Briefly, binding reactions were assembled in a total volume of 10 μL containing 30 nM of double-stranded DNA probe. Binding reactions were performed using the EMSA binding buffer supplied with a commercial EMSA/Gel-Shift assay kit (Beyotime, China), according to the manufacturer's instructions. Purified wild-type OxyR or the mutant OxyR^{S267P} (0, 30, 120, 480, 1920 and 3840 nM) was added at the indicated concentrations, and reactions were incubated at room temperature for 30 min prior to electrophoresis. Protein-DNA complexes were initially resolved on 1.5% native agarose gels prepared in 0.5 × TBE buffer (1 × TBE: 89 mM Tris, 89 mM boric acid, 0.25 mM EDTA) and electrophoresed at 4-5 V/cm under non-denaturing conditions. Based on the concentration ranges determined from agarose-based EMSA, subsequent experiments for comparative analysis of DNA-binding affinity were performed using native polyacrylamide gel electrophoresis (PAGE) for high resolution protein-DNA complexes [45].

2.11. Flow cytometry analysis

To simulate a stress environment, 12 g/L acetate, 2.60 g/L furfural, and 47.36 g/L ethanol was added to RM medium, respectively. After activation, the strains were inoculated into RM and RM with 6% (v/v) ethanol at an initial $OD_{600\ nm}$ of 0.1, followed by cultivation at 30 °C, 100 rpm. Cells in the logarithmic growth phase were collected, washed twice with 1 × PBS, and resuspended in 1 × PBS to a final concentration of 10^7 cells/mL. Cell analysis was performed using flow cytometry on a CytoFLEX flow cytometer with 1 × PBS as the sheath fluid. Fluorescence from EGFP was excited at 488 nm and detected using the FITC channel, opmCherry was excited at 561 nm and detected via the PC5.5 channel. The protocol detail of flow cytometry analytical parameters, and data processing was done as previously described [44]. In addition, the value of EGFP/opmCherry, a normalized ratio to eliminate the internal and external noises that was simplified through (EGFP/OD)/(opmCherry/OD), represented the promoter strength. All experiments were performed with at least three independent biological replicates.

3. Results

3.1. Construction of Z. mobilis ZMNP reverted strain ZMNPC and its fermentation performance under xylose mother liquor

The strain ZMNP carrying the OxyR^{S267P} mutation exhibited improved utilization of xylose mother liquor and lower intracellular ROS levels in different media supplemented with furfural or ethanol as previously reported [42], which was attributed to the upregulation of genes involved in ROS detoxification. In order to confirm this speculation, ZMNP reverted strain ZMNPC was constructed with OxyR^{S267P} reverted to its wild-type allele using native type I–F CRISPR-Cas genome editing system (Fig. 1A). To investigate whether the phenotypic characteristics of strain ZMNPC reverted to those of strain ZM4 after the OxyR^{S267P} mutation was reverted but were different from strain ZMNP, the fermentation performance of strains ZMNPC, ZMNP, and ZM4 were first compared using the xylose mother liquor. The results demonstrated that the reverted strain ZMNPC utilized toxic xylose mother liquor similarly as the wild-type strain ZM4. Both strain ZM4 and strain ZMNPC were less efficient than strain ZMNP with a 20 h lag (Fig. 1B). Additionally, we constructed strain ZM4^{m1} carrying the OxyR^{S267P} mutant in the wild-type strain ZM4. The fermentation performance of ZM4^{m1} in the xylose mother liquor was similar to that of the tolerant strain ZMNP, and its fermentation cycle was shortened by 12 h compared with strain ZM4 (Fig. S1A). These results indicate that the OxyR^{S267P} mutation is the key genetic determinant conferring the strain's tolerance to the hydrolysate.

3.2. Mechanism underlying the xylose mother liquor utilization of ZMNP reverted strain ZMNPC

To examine the effect of OxyR^{S267P} mutation, RNA sequencing was performed on strain ZMNPC and strain ZMNP cultured in RM medium. 165 significantly differentially expressed genes (DEGs) between strain ZMNPC and strain ZMNP (adjust p-value <0.05) were identified through analysis of negative binomial distribution (DESeq2) (Table S4). Among these significantly DEGs, 79 genes were upregulated and 86 downregulated in reverted strain ZMNPC compared to ZMNP. These genes are postulated to participate broadly in cellular processes, and were selected for subsequent functional investigation.

3.2.1. Genes associated with transportation and transcription upregulated in strain ZMNPC

Among the 79 upregulated genes in strain ZMNPC, 12 genes are hypothetical proteins, while the remaining genes were primarily enriched in transcriptional machinery, membrane transport, and central metabolic pathways.

The upregulation of genes encoding ribosomal proteins, including ribosomal protein large subunit proteins (*rplABCDERS*) and small subunit proteins (*rpsCEHNP*), indicated an overall enhancement of translational capacity. *ZMO0368* and *ZMO1327* encoding 6-phosphogluconate dehydratase and HPr family phosphocarrier protein, which were significantly upregulated. The induction of these genes suggests enhancement of central carbon metabolic pathways and activation of sugar uptake and carbon utilization processes. In addition, *ZMO0101* encodes a NAD-dependent epimerase/dehydratase that catalyzes key biochemical transformations, making it crucial for cellular energy metabolism and the modulation of cell surface properties [46,47]. Some genes encode proteins that mediate the transport of various nutrients including amino acids, sugars, and metal ions, and the degradation of complex carbohydrates. For example, *ZMO1049*, *ZMO1591*, and *ZMO1030* encode a permease of ABC transport system, a putative lantabiotic-exporting membrane permease, and a TonB-dependent receptor, respectively. These proteins are collectively involved in the translocation of a wide variety of substrates ranging from ions, sugars, amino acids, vitamins, lipids, antibiotics, and drugs to larger molecules [48,49]. *ZMO1804* encodes amino acid permease responsible for the uptake of amino acids as nutritional sources [50]. *ZMO0025* encodes EamA/RhaT family transporter that participates in an L-cystine/L-cysteine shuttle system, which is suggested to protect the cell membrane under oxidative stress conditions [51]. *nhaA* (*ZMO0119*) encodes Na^+/H^+ antiporter which could enhanced NaAc tolerance of *Z. mobilis* strain [52]. *ZMO0293* encodes sugar transporter responsible for the uptake and metabolism of diverse sugars [53]. Both *zliS* (*ZMO0932*) encoding a secretion-activating factor and *sacB* (*ZMO0374*)

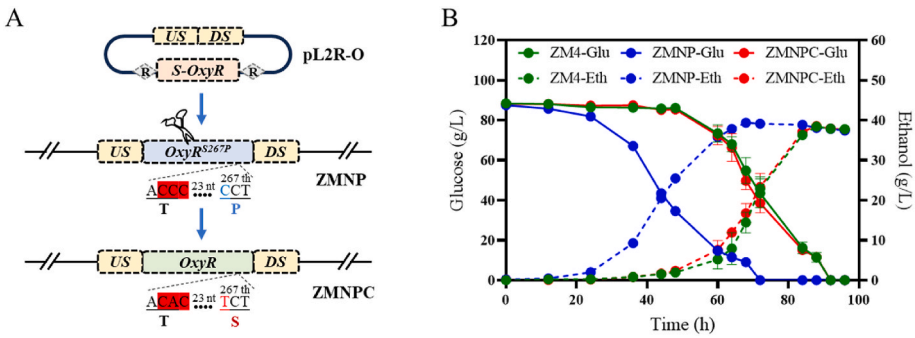

Fig. 1. Construction of the OxyR reverted strain and its performance in toxic xylose mother liquor. The scheme of reverted strain ZMNPC construction by reversion of $OxyR^{S267P}$ to wild-type OxyR in *Z. mobilis* ZMNP using the native type I–F CRISPR system (**A**). The glucose consumption and ethanol production of *Z. mobilis* ZM4, ZMNP, and ZMNPC under xylose mother liquor (**B**). ZM4: wild-type strain *Z. mobilis*, ZMNP: a plasmid-free strain of ZM4 with $OxyR^{S267P}$ mutation, ZMNPC: $OxyR^{S267P}$ reverted strain of ZMNP. All experiments were performed with at least three independent biological replicates.

encoding a levansucrase contribute to the secretion of sucrose hydrolyzing enzymes [54,55].

The coordinated upregulation of transcriptional machinery, central metabolic enzymes, and membrane transport systems under reduced conditions allowing strain ZMNPC to redirect resources from redox defense systems toward anabolic and growth-promoting processes.

3.2.2. Genes associated with general stress responses downregulated in strain ZMNPC

Among the 86 genes downregulated in strain ZMNPC compared to strain ZMNP, which mainly includes enzymes to synthesize cysteine and cellular antioxidants for peroxide removal, to regulate and stabilize intracellular redox potential, as well as to repair proteins, DNA, and RNA.

The inhibitor tolerance capability of strain ZMNPC reduced due to the downregulation of cellular antioxidants compared to that of strain ZMNP. For example, *ZMO1732* (*ahpC*) [56], *ZMO1136* (*mauG*) [42,57], *ZMO1060* (*sod*) [58], and *ZMO1097* (*trx*) [59] that are all related to $O_2\bullet^-$ and H_2O_2 removal were upregulated in ZMNP but downregulated in ZMNPC. *ZMO1211* (*gor*) and *ZMO0753* (*grx*), which function in the interconversion of the intracellular antioxidant glutathione between its reduced (GSH) and oxidized (GSSG) forms, were upregulated in strain ZMNP but downregulated in strain ZMNPC. In addition, the compromise of cysteine biosynthesis in strain ZMNPC could be the reason of the reduced inhibitor tolerance. Cysteine pool is crucial for microorganisms for protein and GSH biosynthesis to defend against inhibitors such as furfural and hydrolysates [60]. Transcriptomic results showed that three genes associated with cysteine synthesis were upregulated in strain ZMNP but downregulated in strain ZMNPC. These genes include *ZMO1685* (*serA1*) and *ZMO1684* (*serC*), responsible for L-serine synthesis, and *ZMO0748* (*cysK*), which catalyzes the final reaction combining O-acetyl-L-serine with H_2S to produce L-cysteine [25]. Downregulation of these genes may decrease the concentration of cysteine in strain ZMNPC, thereby impairing GSH synthesis and thus reducing the scavenging of accumulated ROS and diminishing inhibitor tolerance.

Moreover, the reduced inhibitor tolerance of strain ZMNPC is related to the intracellular redox potential. Transcriptomic results demonstrated that genes *ZMO0256* (*ldh*), *ZMO1753* (*ferredoxin*), *ZMO1113* (*ndh*), *ZMO1571* (*cydA*), and *ZMO1572* (*cydB*), which function in electron transfer and the generation of H_2O from H_2O_2 and O_2 [61], were significantly upregulated in strain ZMNP compared to strain ZM4, but downregulated in strain ZMNPC. The aerobic respiratory chain in microorganisms plays a crucial role in cellular energy production and redox homeostasis, a process closely linked to metabolic activities such as ROS generation and oxidative stress response. By maintaining the intracellular redox potential efficiently, strain ZMNP exhibited strong inhibitor tolerance. In contrast, the downregulation of these genes related to redox balance in strain ZM4 and strain ZMNPC could lead to the reduced inhibitor tolerance capability. Flagellar assembly genes (*flgABM*) were also downregulated, suggesting decreased motility and energy allocation toward non-essential functions under the reduced condition.

Furthermore, the downregulated expression of molecular repair genes in strain ZMNPC may lead to the reduced inhibitor tolerance of strain ZMNPC. Hydroxyl radicals generated by superoxide H_2O_2 can oxidize DNA bases, ribose parts, and proteins, resulting in a variety of damages [62]. The transcriptomic results showed that six genes involved in base excision repair were upregulated in strain ZMNP but downregulated in strain ZMNPC, including *ZMO1401* (*xthA1*) [63], *ZMO1096* (*rnr*) [64], *ZMO1648* (*ung2*) [65], *ZMO1951* (*rraA*) [66], *ZMO1542* (*ssb*) [67], and *ZMO1948* (*ybaK*) that repair the amino acid on the incorrectly charged Cys-tRNAPro [68]. *ZMO1402* encodes the iron-sulfur cluster assembly accessory protein that mediates the repair of oxidatively damaged iron-sulfur cluster modifications in proteins [69]. The downregulation of these genes in strain ZMNPC compared to strain ZMNP thus could reduce the capability of the reverted strain ZMNPC to repair the DNA damages caused by the toxic xylose mother liquor, thereby extending the fermentation duration.

3.2.3. Analysis of the OxyR regulatory network in Z. mobilis

Based on the aforementioned transcriptomic data and the OxyR regulatory network in *E. coli*, a schematic diagram of the potential molecular mechanism of OxyR in *Z. mobilis* was proposed. Genes regulated by OxyR were categorized into the functional groups of antioxidant and cysteine synthesis, redox potential regulation, and repair system. Bacteria employ multiple strategies to counteract oxidative stress. First, they employ a series of ROS-scavenging enzymes to maintain intracellular ROS at low level (Fig. 2A). In addition, the upregulation of cysteine biosynthesis, which is essential for protein and glutathione synthesis under oxidative stress, could help microbial defend ROS for enhanced tolerance [60]. Five genes were upregulated in strain ZMNP. These genes are not known OxyR targets in *E. coli*, likely reflecting distinct metabolic pathways between *E. coli* and *Z. mobilis*. (Fig. 2B). Moreover, the aerobic respiratory chain supports intracellular redox homeostasis and contributes to cellular energy and redox balance, thereby enhancing oxidative stress tolerance (Fig. 2C). Most genes responsible for maintaining intracellular redox potential in *Z. mobilis* lack homologs in *E. coli*, which may be attributed to the distinct respiratory chain structure of *Z. mobilis* [61].Bacteria also activate damage repair systems to restore oxidatively impaired macromolecules including proteins, DNA, and RNA (Fig. 2D). Six genes have been identified that have similar regulatory functions to those in the *E. coli* indicating the conservation of this mechanism for stress tolerance.

Catalase, an enzyme that specifically scavenges H_2O_2, is present in most bacteria. In *E. coli*, the primary H_2O_2-scavenging enzyme is KatG, a

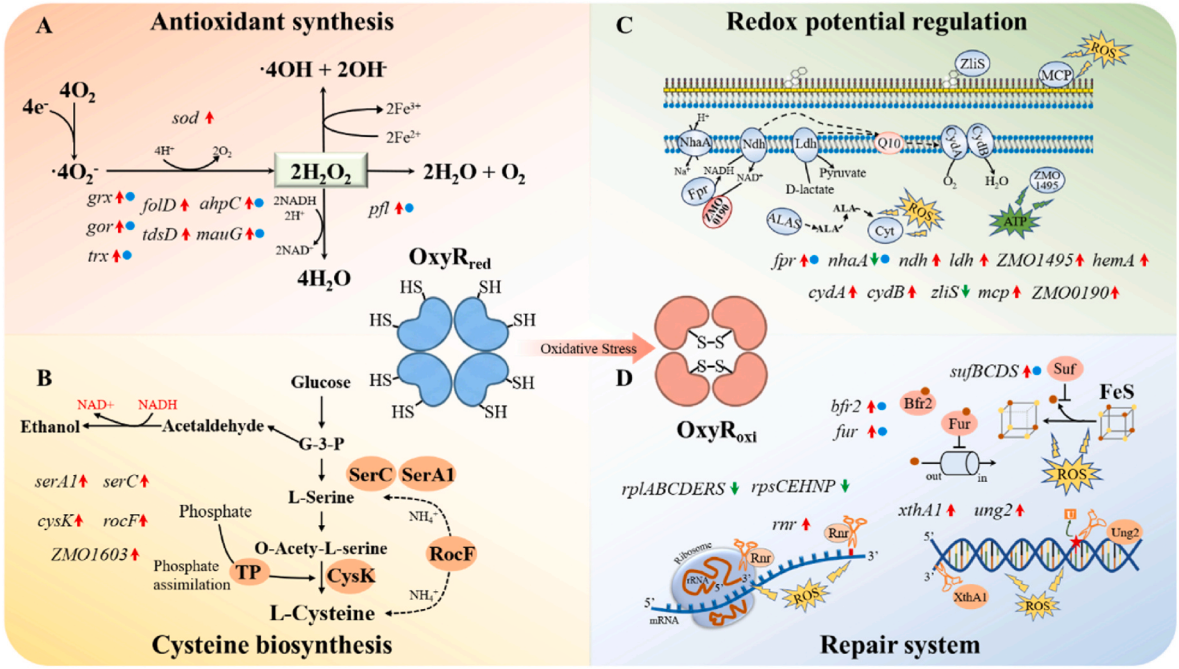

Fig. 2. Potential molecular mechanism of the oxidative stress regulator OxyR. Red arrows indicate upregulated, green arrows indicate downregulated, blue circles indicate that belong to OxyR-regulated in *E. coli*.

protein regulated by OxyR [70]. A homologous protein ZMO1570 (Pfl) in *Z. mobilis* is also upregulated under oxidative stress. The *E. coli* protein YhjA, which converts H_2O_2 to H_2O, is also regulated by OxyR [57]. BLASTP analysis indicates that YhjA shares sequence similarity with ZMO1136 (MauG) [42], implying a potential functional equivalence. NADH peroxidase represents another major class of bacterial H_2O_2-scavenging enzyme. Ahp is typically activated by OxyR [71], and forms a principal system for eliminating excess H_2O_2 together with KatG. While these genes may not be direct OxyR targets, their expression is indirectly upregulated through oxidative stress-induced changes in cellular NADH levels.

Transcriptional comparison of strain ZMNPC and strain ZMNP revealed significant differential expression of genes associated with cysteine synthesis. In *E. coli*, OxyR directly activates enzymes for methionine synthesis [72]. Previous work in *Z. mobilis* demonstrated that cysteine supplementation alleviates furfural or hydrolysate toxicity [25]. Consequently, cysteine synthesis genes may be under OxyR regulation in *Z. mobilis*.

OxyR additionally regulates genes encoding H_2O_2-scavenging enzymes within the thioredoxin and glutathione (GSH) redox systems. These genes exhibit a conserved OxyR-dependent regulatory pattern in both *E. coli* and *Z. mobilis*. Previous work analyzed the expression of these genes in $OxyR^{S267P}$ mutant [42]. Only two genes identified to have same regulatory function in both *E. coli* and *Z. mobilis*. *ZMO0119* (*nhaA*) was downregulated in ZMNP, and its *E. coli* homolog MntH is known to be OxyR-regulated [73]. These proteins primarily maintain the proton motive force to drive cation transport across the plasma membrane. Several genes involved in sensing environmental stress and signal transduction including *ZMO0085* (*mcp*), *ZMO1495*, and *ZMO1198* (*hemA*) were also significantly upregulated in strain ZMNP. *ZMO0190* encodes an RpiR-family transcriptional regulator, a key bacterial protein class often central to carbohydrate metabolism. The downregulation of *ZMO0932* suggests a diminished capacity for sugar hydrolysis and the secretion of hydrolytic enzymes, particularly for sucrose in strain ZMNP. This change coincided with the upregulation of *ZMO0190*. However, further work is needed to evaluate the relationship with OxyR.

Intracellular Fe^{2+} reacts with H_2O_2 via the Fenton reaction to generate HO•, thereby exacerbating oxidative damage. OxyR regulates iron metabolism transcriptionally, primarily by activating the ferric uptake regulator (Fur) to reduce intracellular free iron [72]. *Z. mobilis* ZMO1586 (Bfr2) is a homolog of iron-binding protein Dps that participates in intracellular iron metabolism and directly controlled by OxyR [72]. Under oxidative stress, its expression is upregulated to sequester free iron and inhibit the Fenton reaction. The [4Fe-4S] iron-sulfur cluster at the active site of intracellular dehydrogenases is highly susceptible to ROS, resulting in cluster disintegration and enzyme inactivation. To preserve dehydrogenase activity, OxyR activates the Suf system to repair damaged iron-sulfur centers [74], as evidenced by the upregulation of *sufBCDS* in strain ZMNP. For DNA damage induced by oxidative stress, three genes were upregulated in strain ZMNP to facilitate repair [42].

Based on the higher affinity of oxidized OxyR for the conserved sequence motif ATAGntnnnanCTAT-N7-ATAGntnnnanCTAT, which is the binding motif for OxyR in *E. coli* [17], we performed a targeted genome-wide search for OxyR-specific binding motifs in *Z. mobilis* and *E. coli*. The results showed that 33 of the previously predicted putative OxyR-regulated genes in *Z. mobilis* have orthologs in *E. coli*. Further analysis revealed that the upstream promoter regions of 16 orthologous genes were consistently predicted to contain the conserved OxyR binding motif in both strains (Tables S5–7), suggesting that these 16 genes are likely the core target genes under conserved OxyR-mediated regulation across species.

3.3. The revertant $OxyR^{S267P}$ diminishes oxidative stress tolerance

Cell growth and intracellular ROS levels were assessed after cultivation in RM supplemented with inhibitors such as furfural and ethanol to correlate the relationship between upregulation of ROS detoxification genes and inhibitor tolerance capability of strain ZMNP [42]. Similarly, cell growth and intracellular ROS levels of strain ZMNPC relative to strain ZMNP and strain ZM4 after cultivation in RM supplemented individually with acetate (12 g/L acetate, RMA), furfural (2.6 g/L furfural, RMF), or ethanol (47.36 g/L anhydrous ethanol, RME) were compared in this study.

The results showed that growth curves of the three strains were similar under RM media supplemented with different inhibitors

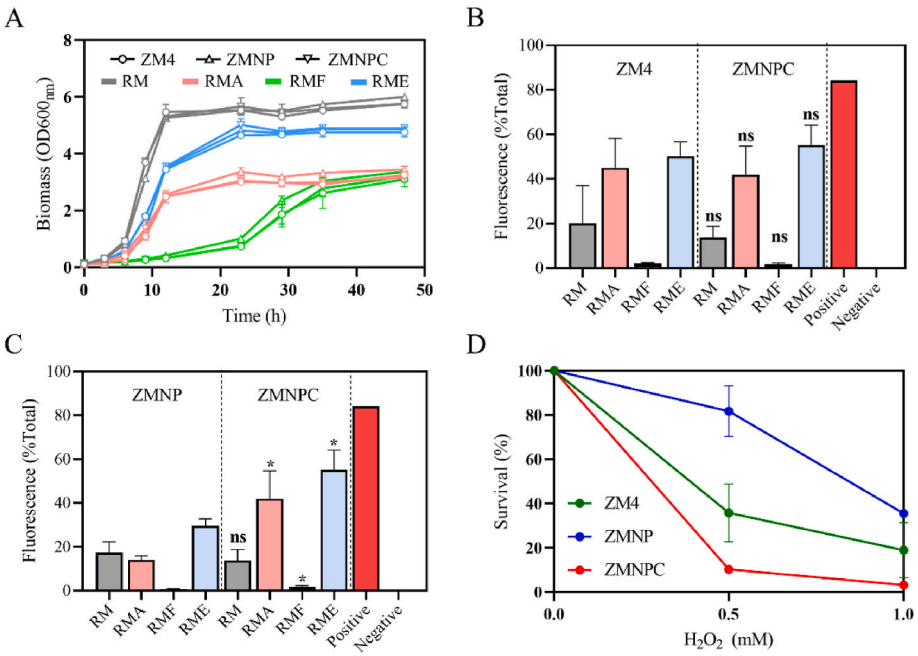

Fig. 3. Cell growth and ROS accumulation of strains ZM4, ZMNP, and ZMNPC responding to different inhibitors. RM and RM supplemented with acetate (RMA), furfural (RMF), and ethanol (RME), were set up to evaluate the growth of strains ZM4, ZMNP, and ZMNPC (**A**). ROS accumulation detection under RM with or without inhibitors (**B, C**). RMA: 12 g/L acetate supplemented in RM media. RMF: 2.60 g/L furfural supplemented in RM media. RME: 47.36 g/L ethanol supplemented in RM media. At least three independent experiments were performed with similar results. Values are the mean of one representative experiment with three technical replicates. Error bars represent standard deviations. T-test analysis was conducted for ROS detection with strain ZM4 or ZMNP as the control. ns represents no significant difference (p-value >0.05), * represents a significant difference (0.01< p-value <0.05). Survival rate of strains ZM4, ZMNP, and ZMNPC after treatment in 0.5 mM and 1 mM H_2O_2 (**D**). All experiments were performed with at least three independent biological replicates.

(Fig. 3A). To assess intracellular ROS levels, cells were harvested 3 h post-inoculation in RM, RMA, RMF, and RME media. Under all inhibitor-supplemented conditions, intracellular ROS levels in strain ZMNPC were comparable to those in strain ZM4, but were significantly higher than in strain ZMNP (Fig. 3B and C). In the basal RM medium, ROS level of strain ZMNPC (17.35%) showed a moderate increase compared to that of strain ZMNP (13.79%), approaching the level observed in strain ZM4 (20.16%). The difference in ROS levels between strains ZMNPC and ZMNP became more pronounced in the presence of inhibitors: ROS levels were significantly elevated in strain ZMNPC compared to strain ZMNP in RMA (41.95% vs. 14.01%), RMF (1.75% vs. 0.64%), and RME (55.17% vs. 29.62%) ($0.01 < p < 0.05$) (Fig. 3C). Moreover, ROS levels in strain ZMNPC were similar to those in strain ZM4 across RMA (45.04%), RMF (2.22%), and RME (50.21%) (Fig. 3B). These results confirm that strain ZMNP maintains lower intracellular ROS levels than both strains ZMNPC and ZM4 under inhibitory conditions.

To further verify that the oxyR^{S267P} mutation reduces intracellular ROS levels in strain ZMNP, we determined the intracellular ROS content of strain ZM4^{m1} under the conditions of different inhibitory additions. The results showed that the intracellular ROS levels of strain ZM4^{m1} were significantly decreased compared with those of the wild-type strain ZM4 when different inhibitors were added (Fig. S1B), demonstrating that the oxyR^{R267P} mutation confers a reduction in intracellular ROS accumulation by upregulating genes associated with oxidative stress responses.

Through its direct binding to OxyR, H_2O_2 induces a conformational change from the reduced to the oxidized form, thereby activating the downstream regulon [21]. Therefore, the effects of peroxide exposure on OxyR^{S267P} reverted strain ZMNPC were examined. A dose-dependent lethality in strains ZMNPC and ZM4 but a mild impact of hydrogen peroxide on the cell survival rate of the strain ZMNP were observed. The strains ZMNPC and ZM4 showed the highest sensitivity to peroxide stress at 0.5 mM H_2O_2 concentration with survival rate of 10.32% and 35.75%, respectively. However, strain ZMNP exhibited only a slight reduction in survival rate (81.72%) (Fig. 3D). At an elevated H_2O_2 concentration of 1 mM, the survival rate of strain ZMNPC dropped to only 3.23%, followed by strain ZM4 at 18.94%, while strain ZMNP still maintained a survival rate of 35.52% (Fig. 3D). These results indicate that strain ZMNP exhibits oxidative stress tolerance to H_2O_2. OxyR^{S267P} mutant facilitating its transition to the oxidized state. This conformational change enhances the expression of downstream antioxidant genes, accelerating intracellular ROS clearance and macromolecular repair, thereby improving strain survival, which is consistent with the results of fatality rate assays conducted after heavy-ion beam [75] and atmospheric and room temperature plasma (ARTP) [76] mutagenesis that cause a decrease in the concentration of intracellular proteins and DNA damage by intracellular ROS accumulation [77–79]. Strain ZMNP exhibited lower fatality than strain ZM4 after 120 Gy heavy-ion irradiation (54.51 ± 5.69% vs. 75.98 ± 7.33%) and 20 s ARTP exposure (100 ± 0.00% vs. 51.89 ± 0.45%) (Table S8).

3.4. *The effect of OxyR mutations on protein structure and DNA-binding affinity*

OxyR was identified as a recurrent mutational target in previous laboratory evolution studies, including in the acidic-pH-tolerant strain 3.6 M [13] and lactate-tolerant strains ZMNP-A, ZMNP-AP, and ZMNP-HAP [22]. OxyR mutation sequences were collected (Table S9) and a multiple sequence alignment was performed using OxyR sequences from 17 experimentally validated bacterial strains to analyze residue conservation and diversity. The results indicated that the wild-type *Z. mobilis* OxyR was identical at 36 aligned amino acid sites with sequence similarity exceeding 70% (represented by colored blocks), reflecting a relatively high degree of conservation (Fig. S2). In contrast, all the observed amino acid substitutions from *Z. mobilis* evolution are not conserved among these sequences (Fig. S2).

The structural information of *E. coli* OxyR (PDB: 1I69) was used to explain the potential effect of OxyR mutations in *Z. mobilis*. The results

between proximity-based analysis of the effect of previously published mutations [21] with known OxyR activity were consistent, which was then proceeded using this analysis pipeline to interpret the outcomes of the $OxyR^{S267P}$ mutant. Using the sequence and structure of *E. coli* OxyR as a reference, the amino acid residues at the OxyR active sites in *Z. mobilis* were analyzed (Table S10). Cys_{204} and Cys_{213} are conserved sites for the formation of intramolecular disulfide bond. The N-terminal region (first 91 aa) of *Z. mobilis* OxyR is structurally undefined in the *E. coli* homolog. Protein structure prediction indicates that in *Z. mobilis* OxyR, residue 7 is spatially close to residues 119, 126, and 129, and residue 50 is close to residues 126 and 129. Mutations T7K and V50A are potentially involved in the conformational transition of the OxyR dimer between its reduced and oxidized states (Fig. S3, Table S11), and the G253D mutant is spatially close to residues 106, 108, 112, 229, and 246 (Fig. 4A, Table S11). Dimerization of oxidized OxyR requires a unique arrangement of prolines (Pro-104, 108, 112, 116) to form a relatively flat helix surface [80]. These results suggest that mutant G253 may support the dimerization of oxidized OxyR by alleviating the requirement of this unique helix arrangement. The redox loop 199–208 is suggested to be required for the tetramerization of reduced OxyR in *E. coli*. The residues 267 and 270 were changed in ZMNP and lactate-evolved strains, are similarly closed to Cys_{204} and Cys_{213} (Fig. 4A). Thus, we proposed that S267P and P270S mutants demonstrate constitutive activity of OxyR due to the destabilization of tetrameric OxyR in its reduced form (Fig. 4A).

Further structural simulation of the *Z. mobilis* OxyR tetramer was conducted to analyze the potential influence of the aforementioned mutation sites on tetramer assembly. The results revealed that, except for residues 267 and 270 located on the exterior surface of the tetramer, the remaining three mutation sites (AA7, AA50, and AA253) are situated at the interface between monomers (Fig. S4), which suggests that these mutations may affect inter-subunit interactions and thereby play a role in modulating tetramer formation and stability. Structural alignment between the reduced and oxidized states of OxyR from *Z. mobilis* and *E. coli* reveals that the loop containing S267 in *Z. mobilis* is positioned closer to the cysteine residues C204 and C213 compared to its counterpart in *E. coli* (Fig. 4B). Notably, the H269 residue is located nearest to the potential disulfide bond formation site according to the predicted structure (Fig. 4B). We propose that this spatial arrangement may introduce steric hindrance to disulfide bond formation in the wild-type protein, potentially slowing its transition from the reduced to the oxidized state and thus delaying oxidative stress responses, while the $OxyR^{S267P}$ mutation could displace H269 away from this region, likely reducing such hindrance and possibly promoting disulfide bond formation and state switching. Thus, we constructed the $OxyR^{H269A}$ mutant strain $ZM4^{m2}$ and determined its intracellular ROS levels with the supplementation of different inhibitors. The substitution of histidine with alanine is expected to reduce steric hindrance primarily due to the markedly smaller side chain of alanine. The experimental results confirmed that the intracellular ROS level of strain $ZM4^{m2}$ was significantly lower than those of strain ZM4 under inhibitory conditions (Fig. S5), which is consistent with the above hypothesis.

Furthermore, molecular dynamics (MD) simulation analysis was performed on the reduced and oxidized forms of wild-type OxyR and its mutant $OxyR^{S267P}$. This analysis focused primarily on the key cysteine sites of C204, C213 and the side chains of the basic residues L265, A266, S/P267, Q268, H269, and P270 in the redox-active loop. In the MD simulations on the reduced form of OxyR that started from the oxidized OxyR (PDB: 1I6A) crystal structure, the wild-type OxyR protein largely maintained the geometric features of the crystal structure, while the $OxyR^{S267P}$ mutation increased the local flexibility of OxyR (Fig. 5A, Table S12). Specifically, the average root-mean-square deviation (RMSD) of wild-type OxyR increased to a maximum of 2.8 Å within 500 frames and then maintained a stable profile until 4000 frames. In contrast, the RMSD of the $OxyR^{S267P}$ mutant peaked at 3.2 Å before decreasing to the level of wild-type OxyR, where it remained stable thereafter (Fig. 5A–Table S12). Upon addition of H_2O_2 to the reaction system, the RMSD values of the $OxyR^{S267P}$ mutant were consistently lower than those of the wild type during the 40 ns simulation. The maximum increases in RMSD of backbone Cα atoms between the crystal structure and the solution structure were approximately 3.6 Å for the mutant and 3.9 Å for the wild type, respectively (Fig. 5B–Table S13). These results indicate that upon binding H_2O_2, the mutant exhibits smaller structural fluctuations and more readily adopts a stable oxidized conformation, which is consistent with an increased probability of forming the stable activating disulfide bond upon oxidative challenge.

Under identical EMSA conditions with a fixed DNA concentration (3 nM), both wild-type OxyR and $OxyR^{S267P}$ mutant were titrated across the same concentration range (0, 120, 480, 1920, and 3840 nM). DNA-protein complexes were observed at lower protein concentrations for $OxyR^{S267P}$ mutant compared to the wild-type OxyR (Fig. 6, Fig. S6). These results indicate that $OxyR^{S267P}$ mutant exhibits enhanced DNA-binding affinity compared with wild-type OxyR under identical conditions.

3.5. Verification of the regulatory capacity of $OxyR^{S267P}$ in response to stress

To verify that the observed changes in gene expression were induced by $OxyR^{S267P}$, we selected three promoters of genes that were DEGs association to the $OxyR^{S267P}$ mutation: the promoter P1753 of gene *fpr* (*ZMO1753*), the promoter P1732 of gene *sod* (*ZMO1732*), and the promoter P1211 of gene *gor* (*ZMO1211*) (Table S4). Using a dual-reporter gene system [44], we then profiled the strength of these promoters and their respective oxidative stress inducibility under RM, RME, RMA, and RMF (Fig. 7A). A strong constitutive promoter P*gap* was used as negative control which is not regulated by OxyR. As expected, promoters P1732 and P1753 in strain ZMNP were strongly induced under the stress of ethanol, acetate and furfural, whereas P1211 was only modestly upregulated under RME, and the native strong promoter P*gap* showed no increase in activity under the ethanol, acetate and furfural supplemented, respectively (Fig. 7B). However, in strain ZMNPC, except for P1732 in RME, the expression levels of P1211 and P1753, as well as the negative control Pgap did not show a significant increase (Fig. 7B).

These results indicate that the global regulator OxyR alters the transcriptional levels of the antioxidant stress-related genes to enable rapid responses and subsequent elimination of the increased ROS induced by inhibitor in the medium. Meanwhile, oxidative stress is a common challenge in industrial microbial fermentation, often frequently generated by high substrate concentration, metabolite accumulation, and exogenous inhibitors [81]. These results demonstrate that the combinations of $OxyR^{S267P}$ with P1732 and P1753, respectively, can serve as biosensors for monitoring oxidative stress induced by ethanol, acetate and furfural. The promoters regulated by OxyR can be utilized to construct broad-spectrum biosensors, which are pivotal for maintaining high and stable production through real-time control of stress-mitigating genes and cellular homeostasis [82,83]. The promoter strengths of P1211 and P1753 were also similar in strain ZMNPC background or higher in strain ZMNP background to that of P*gap* (Fig. 7B), the strongest known promoter in *Z. mobilis* [44], suggesting their potential as strong promoter candidates for metabolic engineering applications.

4. Discussion

This study demonstrated that the S267P mutation in OxyR is the genetic determinant responsible for the enhanced oxidative stress tolerance in the native plasmid-cured *Z. mobilis* derivative strain ZMNP. The $OxyR^{S267P}$ reverted strain ZMNPC had the reduced toxic xylose mother liquor utilization capability (Fig. 1B) and higher intracellular ROS with inhibitor supplementation (Fig. 3B and C). This is consistent with the transcriptomic results that the antioxidant genes and biomolecular repair genes upregulated in strain ZMNP were downregulated in

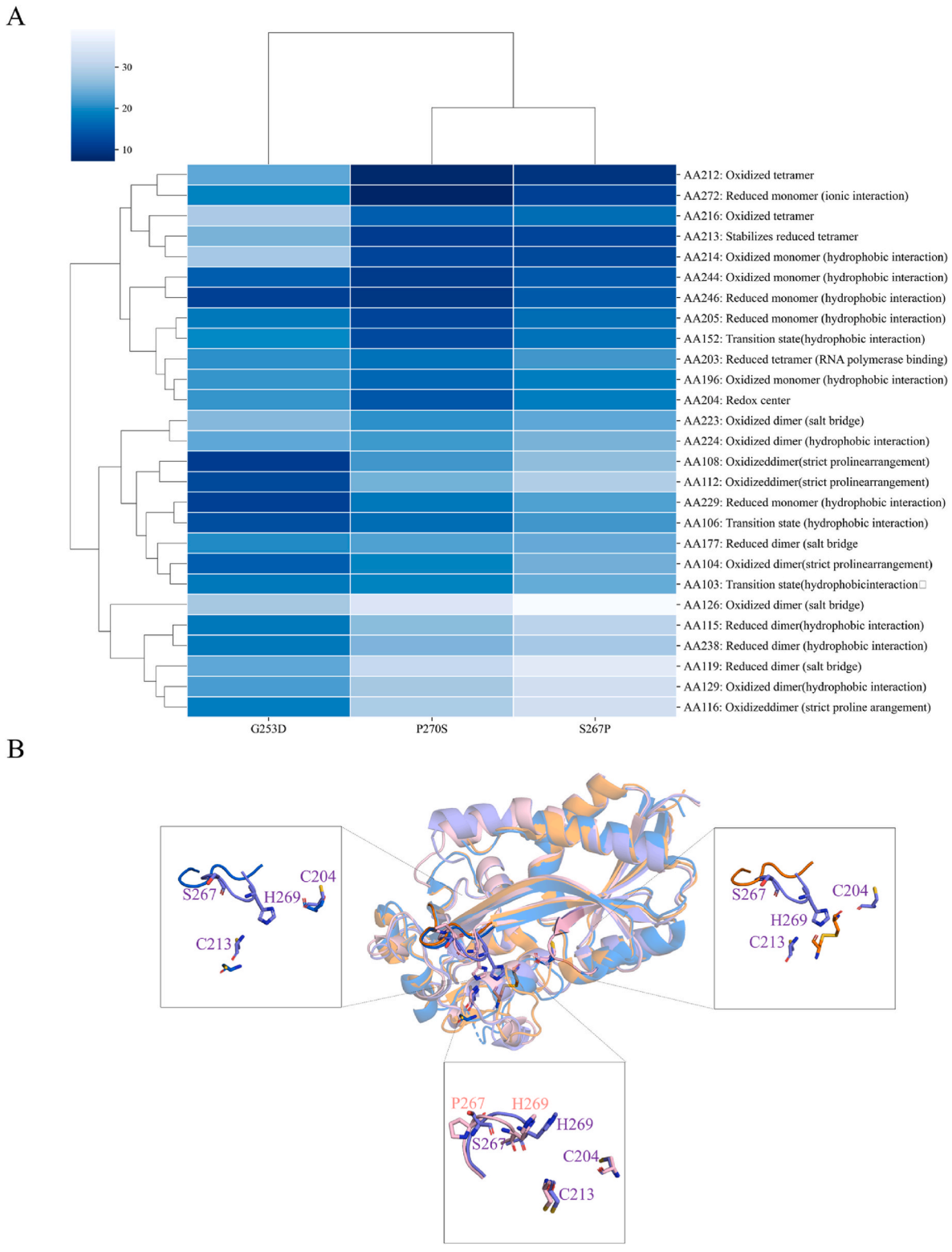

Fig. 4. Potential structural impact of OxyR mutations. Proximity of OxyR mutants to regions of OxyR structural stability (**A**). Distance (Å) between OxyR mutants (columns), and residues involved in OxyR stability (rows) is shown. Potential influence of the S267 mutation on the conformational transition between reduced and oxidized states of *Z. mobilis* OxyR (**B**). The *E. coli* reduced and oxidized forms are shown in blue and orange, respectively. Predicted structures of the *Z. mobilis* wild-type and $OxyR^{S267P}$ mutant are shown in purple and pink, respectively. The residues S267, P267, H269, and the two cysteine residues (C204, C213) have been labeled at their corresponding positions in the structure.

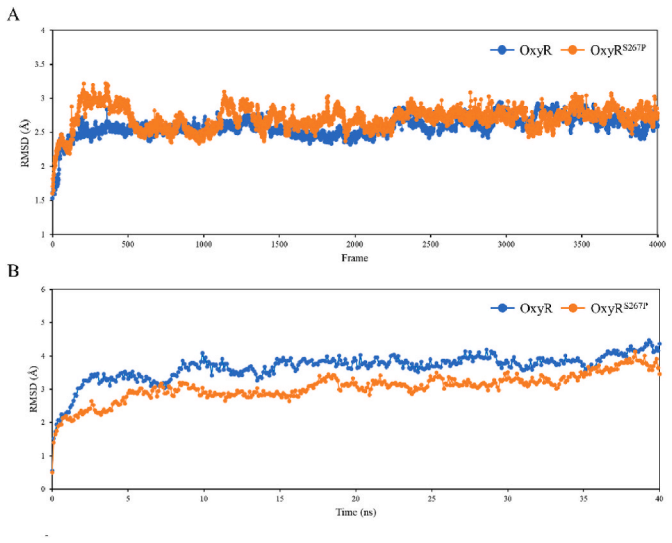

Fig. 5. RMSD (in Å) of the overall structures in OxyR over 4000 simulation frames. The RMSD profiles of reduced form of wild type OxyR and OxyR^{S267P} mutant (**A**). The RMSD profiles of oxidized form of wild type OxyR and OxyR^{S267P} mutant (**B**). In both panels, *Z. mobilis* wild type OxyR and the OxyR^{S267P} mutant are represented by blue and orange curves, respectively.

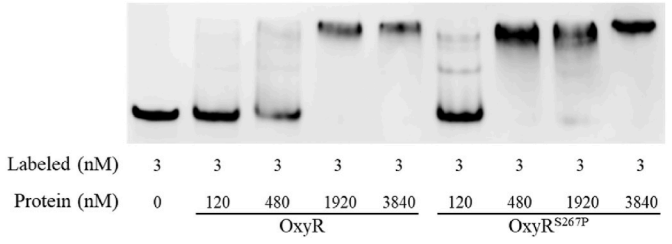

Fig. 6. DNA-binding affinity of the OxyR protein. EMSA was performed using a constant concentration of labeled DNA and increasing concentrations of wild-type OxyR and OxyR^{S267P} mutant proteins. All reactions were conducted under identical experimental conditions.

strain ZMNPC (Table S4). It is hypothesized that the S267P mutation likely leads to a constitutively active OxyR protein, which perpetually primes the antioxidant defense system even in the absence of stress. And the better xylose mother liquor utilization and lower intracellular ROS of OxyR^{S267P} mutant strain ZM4^{m1} (Fig. S1), which also verifies the above hypothesis.

The OxyR regulatory mechanism has been well characterized in *E. coli* [19], which typically senses H_2O_2 and undergoes conformational changes to enable binding to the promoter regions of downstream target genes, thereby activating or repressing their expression. These target genes are not only involved in the oxidative stress response, but also associated with other physiological processes such as iron uptake, Fe–S cluster assembly and repair, heme biosynthesis, and sRNA regulation [20,84,85]. In this study, we confirmed through reverse genetics that OxyR primarily regulates antioxidant genes such as *ahpC*, *gor*, *grx*, *mauG*, *sod*, *trx*, *ldh*, *fpr*, *ndh*, *cydA/B*, *cysK*, *serC*, and *serA1*, and the biomolecular repair genes such as *xthA1*, *rnr*, and *ung2* in *Z. mobilis* (Fig. 2, Table S4). And the motif while essential antioxidant and repair functions remain largely similar [12,86,87], key divergences are evident in redox homeostasis and metabolic regulation. Specifically, the lack of *E. coli* homologs among many *Z. mobilis* redox-balancing genes likely reflects adaptations to its unique respiration chain and ED pathway (Fig. 2C). The observed differential expression of carbohydrate metabolism and stress-sensing genes lacks confirmed direct OxyR regulation thus indicating a more integrated and possibly indirect regulatory role for OxyR in coordinating these responses (Fig. 2C). Our findings thus expand the known functional scope of OxyR and provide a refined framework and key targets for exploring its regulatory role across diverse microorganisms.

The evolutionary adaptation of bacteria to environmental stress is governed by a fundamental "fear-versus-greed" trade-off between stress tolerance ("fear") and rapid growth ("greed"), as limited cellular resources preclude their simultaneous optimization [88]. This pattern is consistently observed in evolution experiments with various bacteria. For instance, *E. coli* mutants evolved for high iron tolerance, which exhibit improved growth under iron stress and harbor mutations in the oxidative stress regulator OxyR, showed lower growth in the stress-free environment [21]. This observation demonstrates that their investment in stress tolerance incurs a cost to normal growth. Similarly, *Z. mobilis* mutants with *oxyR* mutations, evolved for tolerance to acidic pH or lactate, also display growth defects in stress-free environment [13,22], further validating the universality of this trade-off. Contrasting with the typical trade-off, the growth under both normal and stress-free conditions of strain ZMNP is similar to that of the wild-type (Fig. 3A), yet it maintains significantly lower intracellular ROS levels under stress (Fig. 3B and C). We hypothesize that the applied stress may be of insufficient intensity to trigger a costly resource reallocation. As a result, the required investment in stress tolerance remains minimal and does not encroach upon growth resources. This indicates that the trade-off is stress-level-dependent, cells may enhance cellular efficiency to mitigate oxidative damage under mild stress, thereby maintaining fitness without apparent growth cost.

The strain ZMNP containing OxyR^{S267P} mutation not only reduces intracellular ROS levels under inhibitor-induced stress but also significantly decreases the lethality of heavy-ion beam and ARTP mutagenesis (Table S8). Although the mechanisms of ROS accumulation differ between environmental inhibitors and physical mutagenesis—the former indirectly generates superoxide anions via metabolic disruption [89], while the latter directly produces •OH or exogenous ROS/RNS [79,90]—the antioxidant genes regulated by OxyR^{S267P} can effectively scavenge ROS from these distinct sources. However, during mutagenesis breeding, this rapid ROS clearance may act as a double-edged sword by prematurely removing key reactive species such as •OH, which is responsible for DNA strand breaks. This reduction in DNA damage consequently weakens mutagenic efficiency and leads to insufficient mutational diversity and complicates the construction of high-quality mutant libraries and the screening of desired phenotypic variants.

It is a common occurrence for genetic changes in *oxyR* to adaptation to oxidative stress. In addition to the OxyR^{S267P} of *Z. mobilis* in this study, it is reported different types of OxyR mutations in *Z. mobilis* and other microorganisms [13,21,22,42]. Mutations in OxyR typically cluster in the central third of the protein, a domain housing critical redox-active sites for its monomeric or tetrameric forms [21]. However, we identified two mutations T7K and V50A within the 91 N-terminal amino acids of *Z. mobilis* OxyR, a region absent in the *E. coli* homolog. Their location in this atypical region suggests a potentially specialized function that requires future investigation. Our structural model suggested that the S267P mutation primarily functions for alleviating steric hindrance near the disulfide bond-forming cysteines (C_{204}–C_{213}) (Fig. 4B). We performed site-directed mutagenesis at the H269 site to generate the OxyR^{H269A} mutant strain. The intracellular ROS level of this mutant was significantly decreased (Fig. S5), verifying that alleviating steric hindrance at this position alone is sufficient to recapitulate the enhanced ROS scavenging capacity conferred by the S267P mutation. The functional impact of recurrent mutations T7K, V50A, and G253D, while not directly altering the redox-active site, was likely positioned to modulate the stability equilibrium between the reduced tetramer and the oxidized dimer. By integrating structural modeling (Fig. 4), molecular dynamics simulations (Fig. 5), and EMSA experiments (Fig. 6, Fig. S6), these results collectively support a model in which the mutation modulates the structural and dynamic properties of OxyR, leading to enhanced

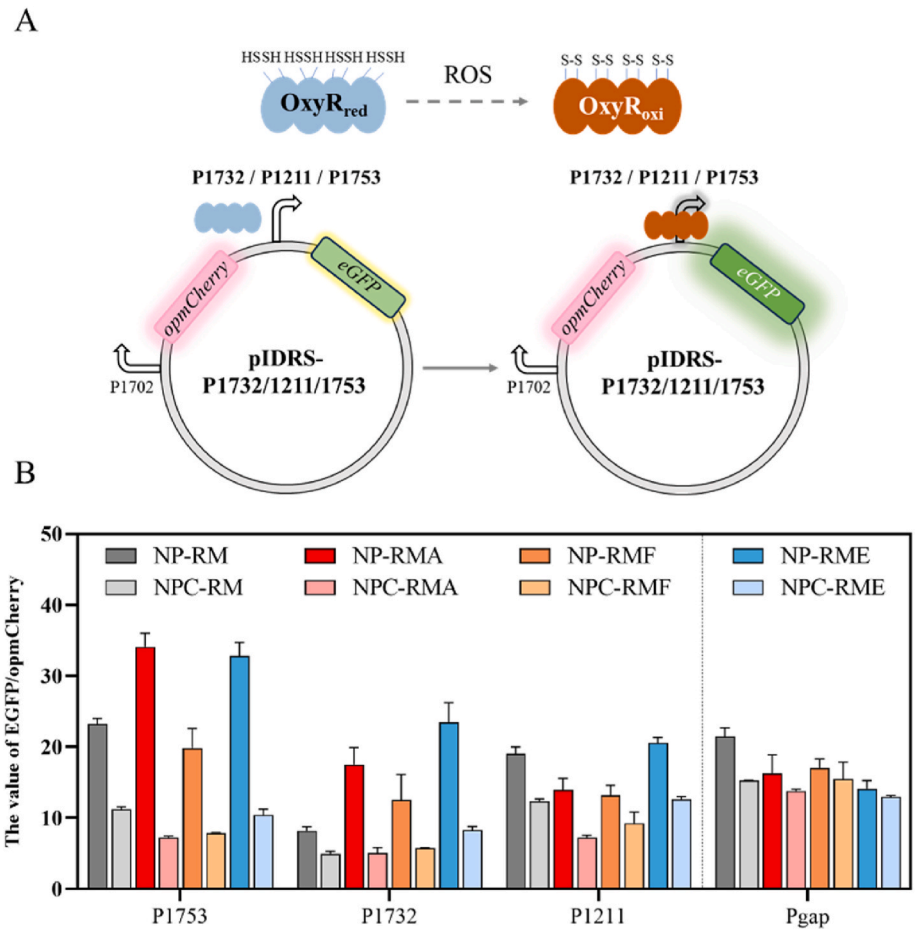

Fig. 7. The quantification of promoter strengths of OxyR regulons by dual reporter-gene system with the induction of ethanol, acetate, or furfural supplementation. The *opmCherry* gene is driven by the constitutive promoter P1702, while *eGFP* is under the control of the test promoters (P1732, P1211, or P1753). Upon intracellular oxidative stress (e.g., H_2O_2), the reduced form of OxyR (OxyR$_{red}$) undergoes oxidation to form OxyR$_{oxi}$, which enables its binding to the target promoter and subsequent activation of EGFP expression (**A**). The relative strength of promoter is a calibrated strength that the value of EGFP/opmCherry (**B**). NP: ZMNP strain with OxyR^{S267P} mutant, NPC: ZMNPC strain with OxyR^{S267P} revertant mutant, RM: RMG5 medium, RMA: 12 g/L acetate supplemented in RM media, RMF: 2.60 g/L furfural supplemented in RM media, RME: 47.36 g/L ethanol supplemented in RM media. P1702: native constitutive promoter in *Z. mobilis*, P*gap*: native strong promoter in *Z. mobilis*, P1211: the promoter of *ZMO1211*, P1732: the promoter of *ZMO1732*, P1753: the promoter of *ZMO1753*. All experiments were performed with at least three independent biological replicates.

DNA-binding affinity.

In this study, the regulatory capacity of OxyR on several antioxidant stress-related genes was further validated. OxyR^{S267P} had the potential to be developed as a metabolic engineering tool to monitor or mitigate intracellular ROS. The OxyR^{S267P} mutation constitutes a valuable genetic target for metabolic engineering, enabling the construction of industrial strains with broad-spectrum tolerance to toxic inhibitors present in lignocellulosic hydrolysates. In addition, the OxyR-regulated genetic elements P1732 and P1753 function as highly effective biosensors characterized by strong basal strength and high inducibility (Fig. 7). These tools not only allow for real-time monitoring of cellular stress during fermentation but also pave the way for constructing dynamic genetic circuits that autonomously activate stress-mitigating genes in response to ROS accumulation, thereby enabling more intelligent and efficient biomanufacturing processes [91,92].

5. Conclusion

In this study, site-directed reversion mutagenesis was performed on OxyR^{S267P} in the hydrolysate-tolerant mutant strain ZMNP to construct the reverted strain ZMNPC. Functional validation confirmed that the OxyR^{S267P} mutation enhanced hydrolysate tolerance and post-mutagenesis survival rate in *Z. mobilis*. Mechanistic investigations revealed that the OxyR^{S267P} mutation likely reduced the steric hindrance for disulfide bond formation, facilitating the conversion of OxyR to its oxidized state and thereby activating downstream antioxidant stress genes to rapidly scavenge intracellular ROS. Based on the properties of OxyR^{S267P}, intracellular ROS-responsive biosensors were developed, which exhibited responses to multiple inhibitors including acetate, furfural, and ethanol, enabling real-time monitoring of intracellular oxidative stress during cell growth. Nevertheless, the precise regulatory network of the *Z. mobilis* OxyR and its detailed protein molecular mechanism remain to be experimentally elucidated in future work, which will provide genetic targets and biological parts for constructing stress-tolerant industrial strains.

CRediT authorship contribution statement

Yi Wang: Writing – review & editing, Writing – original draft, Validation, Methodology, Investigation, Formal analysis, Data curation. **Binan Geng:** Writing – review & editing, Writing – original draft, Visualization, Validation, Methodology, Formal analysis, Data curation. **Shuyi Liu:** Investigation, Formal analysis, Data curation. **Yalun Wu:** Visualization, Software, Methodology, Data curation. **Shihui Yang:** Writing – review & editing, Writing – original draft, Visualization, Supervision, Resources, Project administration, Funding acquisition,

Formal analysis, Data curation, Conceptualization.

Funding

This work was supported by the National Key Research and Development Program of China (2022YFA0911800 to S.Y.), the International Science and Technology Cooperation base of Hubei Province (SH2318 to S.Y.), the Innovation Base for Introducing Talents of Discipline of Hubei Province (2019BJH021 to S.Y.), and the Technology Achievement Transformation Project of Wuhan Science and Technology Innovation Bureau (2024030803010187 to S.Y.).

Declaration of competing interest

The authors declare the following financial interests/personal relationships which may be considered as potential competing interests: There is patent application associated with this study, and Shihui YANG is the founder of Wuhan ZymoBiotech Inc.

Appendix A. Supplementary data

Supplementary data to this article can be found online at https://doi.org/10.1016/j.synbio.2026.03.010.

References

[1] Seib KL, Wu HJ, Srikhanta YN, Edwards JL, Falsetta ML, Hamilton AJ, Maguire TL, Grimmond SM, Apicella MA, McEwan AG, Jennings MP. Characterization of the OxyR regulon of *Neisseria gonorrhoeae*. Mol Microbiol 2007;63:54–68. https://doi.org/10.1111/j.1365-2958.2006.05478.x.

[2] Birben E, Sahiner UM, Sackesen C, Erzurum S, Kalayci O. Oxidative stress and antioxidant defense. World Allergy Organ J 2012;5:9–19. https://doi.org/10.1097/WOX.0b013e3182439613.

[3] Imlay JA. Pathways of oxidative damage. Annu Rev Microbiol 2003;57:395–418. https://doi.org/10.1146/annurev.micro.57.030502.090938.

[4] Storz G, Tartaglia LA. OxyR: a regulator of antioxidant genes. J Nutr 1992;122:627–30. https://doi.org/10.1093/jn/122.suppl_3.627.

[5] Yu Z, Xu Z, Zeng R, Xu M, Zheng H, Huang D, Weng Z, Tang D. D-Band-Center-Engineered platinum-based nanozyme for personalized pharmacovigilance. Angew Chem Int Ed Engl 2025;64:e202414625. https://doi.org/10.1002/anie.202414625.

[6] Yu Z, Xu Z, Zeng R, Xu M, Zou M, Huang D, Weng Z, Tang D. Tailored metal-organic framework-based nanozymes for enhanced enzyme-like catalysis. Angew Chem Int Ed Engl 2025;64:e202420200. https://doi.org/10.1002/anie.202420200.

[7] Cornelis P, Wei Q, Andrews SC, Vinckx T. Iron homeostasis and management of oxidative stress response in bacteria. Metallomics 2011;3:540–9. https://doi.org/10.1039/c1mt00022e.

[8] Wu Y, Vulic M, Keren I, Lewis K. Role of oxidative stress in persister tolerance. Antimicrob Agents Chemother 2012;56:4922–6. https://doi.org/10.1128/AAC.00921-12.

[9] Henderson IR, Owen P. The major phase-variable outer membrane protein of *Escherichia coli* structurally resembles the immunoglobulin A1 protease class of exported protein and is regulated by a novel mechanism involving Dam and oxyR. J Bacteriol 1999;181:2132–41. https://doi.org/10.1128/JB.181.7.2132-2141.1999.

[10] Melstrom Jr KA, Kozlowski R, Hassett DJ, Suzuki H, Bates DM, Gamelli RL, Shankar R. Cytotoxicity of *Pseudomonas* secreted exotoxins requires OxyR expression. J Surg Res 2007;143:50–7. https://doi.org/10.1016/j.jss.2007.02.046.

[11] Lau GW, Britigan BE, Hassett DJ. *Pseudomonas aeruginosa* OxyR is required for full virulence in rodent and insect models of infection and for resistance to human neutrophils. Infect Immun 2005;73:2550–3. https://doi.org/10.1128/IAI.73.4.2550-2553.2005.

[12] Teramoto H, Inui M, Yukawa H. OxyR acts as a transcriptional repressor of hydrogen peroxide-inducible antioxidant genes in *Corynebacterium glutamicum* R. FEBS J 2013;280:3298–312. https://doi.org/10.1111/febs.12312.

[13] Yang Q, Yang Y, Tang Y, Wang X, Chen Y, Shen W, Zhan Y, Gao J, Wu B, He M, et al. Development and characterization of acidic-pH-tolerant mutants of *Zymomonas mobilis* through adaptation and next-generation sequencing-based genome resequencing and RNA-Seq. Biotechnol Biofuels 2020;13:144. https://doi.org/10.1186/s13068-020-01781-1.

[14] Kim SO, Merchant K, Nudelman R, Beyer WF, Keng T, DeAngelo J, Hausladen A, Stamler JS. OxyR: a molecular code for redox-related signaling. Cell 2002;109:383–96. https://doi.org/10.1016/s0092-8674(02)00723-7.

[15] Aslund F, Zheng M, Beckwith J, Storz G. Regulation of the OxyR transcription factor by hydrogen peroxide and the cellular thiol-disulfide status. Proc Natl Acad Sci U S A 1999;96:6161–5. https://doi.org/10.1073/pnas.96.11.6161.

[16] Zheng M, Åslund F, Storz G. Activation of the OxyR transcription factor by reversible disulfide bond formation. Science 1998;279:1718–22. https://doi.org/10.1126/science.279.5357.1718.

[17] Toledano MB, Kullik I, Trinh F, Baird PT, Schneider TD, Storz G. Redox-dependent shift of OxyR-DNA contacts along an extended DNA-binding site: a mechanism for differential promoter selection. Cell 1994;78:897–909. https://doi.org/10.1016/s0092-8674(94)90702-1.

[18] Jo I, Chung IY, Bae HW, Kim JS, Song S, Cho YH, Ha NC. Structural details of the OxyR peroxide-sensing mechanism. Proc Natl Acad Sci U S A 2015;112:6443–8. https://doi.org/10.1073/pnas.1424495112.

[19] Chiang SM, Schellhorn HE. Regulators of oxidative stress response genes in *Escherichia coli* and their functional conservation in bacteria. Arch Biochem Biophys 2012;525:161–9. https://doi.org/10.1016/j.abb.2012.02.007.

[20] Zheng M, Wang X, Doan B, Lewis KA, Schneider TD, Storz G. Computation-directed identification of OxyR DNA binding sites in *Escherichia coli*. J Bacteriol 2001;183:4571–9. https://doi.org/10.1128/JB.183.15.4571-4579.2001.

[21] Anand A, Chen K, Catoiu E, Sastry AV, Olson CA, Sandberg TE, Seif Y, Xu S, Szubin R, Yang L, et al. OxyR is a convergent target for mutations acquired during adaptation to oxidative stress-prone metabolic states. Mol Biol Evol 2020;37:660–7. https://doi.org/10.1093/molbev/msz251.

[22] Hu MM, Chen YH, Geng BN, Yan XY, Wu YL, Peng QQ, Chen JH, Hu W, He QN, Yang SH. Engineering strategies and tolerance mechanisms for robust d-lactate producer development of *Zymomonas mobilis*. Bioresour Technol 2026;440. https://doi.org/10.1016/j.biortech.2025.133521.

[23] Wang X, He Q, Yang Y, Wang J, Haning K, Hu Y, Wu B, He M, Zhang Y, Bao J, et al. Advances and prospects in metabolic engineering of *Zymomonas mobilis*. Metab Eng 2018;50:57–73. https://doi.org/10.1016/j.ymben.2018.04.001.

[24] Yang S, Fei Q, Zhang Y, Contreras LM, Utturkar SM, Brown SD, Himmel ME, Zhang M. *Zymomonas mobilis* as a model system for production of biofuels and biochemicals. Microb Biotechnol 2016;9:699–717. https://doi.org/10.1111/1751-7915.12408.

[25] Yan X, Wang X, Yang Y, Wang Z, Zhang H, Li Y, He Q, Li M, Yang S. Cysteine supplementation enhanced inhibitor tolerance of *Zymomonas mobilis* for economic lignocellulosic bioethanol production. Bioresour Technol 2022;349:126878. https://doi.org/10.1016/j.biortech.2022.126878.

[26] Wu B, Qin H, Yang Y, Duan G, Yang S, Xin F, Zhao C, Shao H, Wang Y, Zhu Q, et al. Engineered *Zymomonas mobilis* tolerant to acetic acid and low pH via multiplex atmospheric and room temperature plasma mutagenesis. Biotechnol Biofuels 2019;12:10. https://doi.org/10.1186/s13068-018-1348-9.

[27] Li R, Shen W, Yang Y, Du J, Li M, Yang S. Investigation of the impact of a broad range of temperatures on the physiological and transcriptional profiles of *Zymomonas mobilis* ZM4 for high-temperature-tolerant recombinant strain development. Biotechnol Biofuels 2021;14:146. https://doi.org/10.1186/s13068-021-02000-1.

[28] Vriesekoop F, Pamment NB. Acetaldehyde stimulation of the growth of *Zymomonas mobilis* subjected to ethanol and other environmental stresses: effect of other metabolic electron acceptors and evidence for a mechanism. Fermentation 2021;7:80. https://doi.org/10.3390/fermentation7020080.

[29] Hu M, Bao W, Peng Q, Hu W, Yang X, Xiang Y, Yan X, Li M, Xu P, He Q, Yang S. Metabolic engineering of *Zymomonas mobilis* for co-production of D-lactic acid and ethanol using waste feedstocks of molasses and corncob residue hydrolysate. Front Bioeng Biotechnol 2023;11:1135484. https://doi.org/10.3389/fbioe.2023.1135484.

[30] Uhlenbusch I, Sahm H, Sprenger GA. Expression of an L-alanine dehydrogenase gene in *Zymomonas mobilis* and excretion of L-alanine. Appl Environ Microbiol 1991;57:1360–6. https://doi.org/10.1128/aem.57.5.1360-1366.1991.

[31] Yang S, Mohagheghi A, Franden MA, Chou YC, Chen X, Dowe N, Himmel ME, Zhang M. Metabolic engineering of *Zymomonas mobilis* for 2,3-butanediol production from lignocellulosic biomass sugars. Biotechnol Biofuels 2016;9:189. https://doi.org/10.1186/s13068-016-0606-y.

[32] Wang Z, Wang X, Yan X, Yi H, He S, Zhang H, Zhou X, He Q, Yang S. Metabolic engineering of an industrial bacterium *Zymomonas mobilis* for anaerobic L-serine production. Synth Syst Biotechnol 2024;9:349–58. https://doi.org/10.1016/j.synbio.2024.03.008.

[33] Bao W, Shen W, Peng Q, Du J, Yang S. Metabolic engineering of *Zymomonas mobilis* for acetoin production by carbon redistribution and cofactor balance. Fermentation 2023;9. https://doi.org/10.3390/fermentation9020113.

[34] Qiu M, Shen W, Yan X, He Q, Cai D, Chen S, Wei H, Knoshaug EP, Zhang M, Himmel ME, Yang S. Metabolic engineering of *Zymomonas mobilis* for anaerobic isobutanol production. Biotechnol Biofuels 2020;13:15. https://doi.org/10.1186/s13068-020-1654-x.

[35] Khandelwal R, Srivastava P, Bisaria VS. Expression of *Escherichia coli* malic enzyme gene in *Zymomonas mobilis* for production of malic acid. J Biotechnol 2022;351:23–9. https://doi.org/10.1016/j.jbiotec.2022.04.007.

[36] He Y, Wu B, Xia W, Zhao KY, Qin Y, Tan Q, Yu QH, Liu PT, Hu GQ, He MX. Metabolic engineering of *Zymomonas moblis* for ethylene production from straw hydrolysate. Appl Microbiol Biotechnol 2021;105:1709–20. https://doi.org/10.1007/s00253-021-11091-7.

[37] Li Y, Wang Y, Wang RX, Yan XY, Wang JW, Wang X, Chen SW, Bai FW, He QN, Yang SH. Metabolic engineering of *Zymomonas mobilis* for continuous co-production of bioethanol and poly-3-hydroxybutyrate (PHB). Green Chem 2022;24:2588–601. https://doi.org/10.1039/d1gc04522a.

[38] Liu Y, Cruz-Morales P, Zargar A, Belcher MS, Pang B, Englund E, Dan Q, Yin K, Keasling JD. Biofuels for a sustainable future. Cell 2021;184:1636–47. https://doi.org/10.1016/j.cell.2021.01.052.

[39] Matsushita K, Azuma Y, Kosaka T, Yakushi T, Hoshida H, Akada R, Yamada M. Genomic analyses of thermotolerant microorganisms used for high-temperature fermentations. Biosci Biotechnol Biochem 2016;80:655–68. https://doi.org/10.1080/09168451.2015.1104235.
[40] He MX, Wu B, Shui ZX, Hu QC, Wang WG, Tan FR, Tang XY, Zhu QL, Pan K, Li Q, Su XH. Transcriptome profiling of *Zymomonas mobilis* under furfural stress. Appl Microbiol Biotechnol 2012;95:189–99. https://doi.org/10.1007/s00253-012-4155-4.
[41] Yang SH, Franden MA, Wang X, Chou YC, Hu Y, Brown SD, Pienkos PT, Zhang M. Transcriptomic profiles of *Zymomonas mobilis* 8b to furfural acute and long-term stress in both glucose and xylose conditions. Front Microbiol 2020;11:13. https://doi.org/10.3389/fmicb.2020.00013.
[42] Geng B, Liu S, Chen Y, Wu Y, Wang Y, Zhou X, Li H, Li M, Yang S. A plasmid-free *Zymomonas mobilis* mutant strain reducing reactive oxygen species for efficient bioethanol production using industrial effluent of xylose mother liquor. Front Bioeng Biotechnol 2022;10:1110513. https://doi.org/10.3389/fbioe.2022.1110513.
[43] Zheng YL, Han JM, Wang BY, Hu XY, Li RX, Shen W, Ma XD, Ma LX, Yi L, Yang SH, Peng WF. Characterization and repurposing of the endogenous Type I-F CRISPR-Cas system of *Zymomonas mobilis* for genome engineering. Nucleic Acids Res 2019;47:11461–75. https://doi.org/10.1093/nar/gkz940.
[44] Yang YF, Shen W, Huang J, Li RX, Xiao YB, Wei H, Chou YC, Zhang M, Himmel ME, Chen SW, et al. Prediction and characterization of promoters and ribosomal binding sites of *Zymomonas mobilis* in system biology era. Biotechnol Biofuels 2019;12:52. https://doi.org/10.1186/s13068-019-1399-6.
[45] Ream JA, Lewis LK, Lewis KA. Rapid agarose gel electrophoretic mobility shift assay for quantitating protein: RNA interactions. Anal Biochem 2016;511:36–41. https://doi.org/10.1016/j.ab.2016.07.027.
[46] Rehman AU, Hamza MA, Liu F, Zhang L, Ma Y, Wang D, Chen Z. NAD-dependent epimerase/dehydratase serves as a novel potential target for fluoxastrobin in *Pestalotiopsis trachicarpicola*, the causal agent of tea foliar disease. Phytopathology 2025;115:794–808. https://doi.org/10.1094/phyto-11-24-0357-r.
[47] Islam R, Brown S, Taheri A, Dumenyo CK. The gene encoding NAD-dependent epimerase/dehydratase, wcaG, affects cell surface properties, virulence, and extracellular enzyme production in the soft rot phytopathogen, *Pectobacterium carotovorum*. Microorganisms 2019;7. https://doi.org/10.3390/microorganisms7060172.
[48] Biemans-Oldehinkel E, Doeven MK, Poolman B. ABC transporter architecture and regulatory roles of accessory domains. FEBS Lett 2005;580:1023–35. https://doi.org/10.1016/j.febslet.2005.11.079.
[49] Fujita M, Mori K, Hara H, Hishiyama S, Kamimura N, Masai E. A TonB-dependent receptor constitutes the outer membrane transport system for a lignin-derived aromatic compound. Commun Biol 2019;2:432. https://doi.org/10.1038/s42003-019-0676-z.
[50] Ray SC, Shen Q, Rappleye CA. Three transporters, including the novel Gai1 permease, drive amino acid uptake in *Histoplasma* yeasts. Virulence 2024;15:2438750. https://doi.org/10.1080/21505594.2024.2438750.
[51] Ahmad R, Gastoldi G, Wong S-T, Baeza Garcia A, Caljon G. The EamA metabolite transporter does not affect antileishmanial drug susceptibility. Int J Parasitol Drugs Drug Resist 2026;30:100632. https://doi.org/10.1016/j.ijpddr.2026.100632.
[52] Yang S, Land ML, Klingeman DM, Pelletier DA, Lu TY, Martin SL, Guo HB, Smith JC, Brown SD. Paradigm for industrial strain improvement identifies sodium acetate tolerance loci in *Zymomonas mobilis* and *Saccharomyces cerevisiae*. Proc Natl Acad Sci U S A 2010;107:10395–400. https://doi.org/10.1073/pnas.0914506107.
[53] Tamayo E, Nada B, Hafermann I, Benz JP. Correlating sugar transporter expression and activities to identify transporters for an orphan sugar substrate. Appl Microbiol Biotechnol 2024;108:83. https://doi.org/10.1007/s00253-023-12907-4.
[54] Kondo Y, Toyoda A, Fukushi H, Yanase H, Tonomura K, Kawasaki H, Sakai T. Cloning and characterization of a pair of genes that stimulate the production and secretion of *Zymomonas mobilis* extracellular levansucrase and invertase. Biosci Biotechnol Biochem 1994;58:526–30. https://doi.org/10.1271/bbb.58.526.
[55] Gunasekaran P, Karunakaran T, Cami B, Mukundan AG, Preziosi L, Baratti J. Cloning and sequencing of the *sacA* gene: characterization of a sucrase from *Zymomonas mobilis*. J Bacteriol 1990;172:6727–35. https://doi.org/10.1128/jb.172.12.6727-6735.1990.
[56] Mongkolsuk S, Whangsuk W, Vattanaviboon P, Loprasert S, Fuangthong M. A *Xanthomonas* alkyl hydroperoxide reductase subunit C (*ahpC*) mutant showed an altered peroxide stress response and complex regulation of the compensatory response of peroxide detoxification enzymes. J Bacteriol 2000;182:6845–9. https://doi.org/10.1128/JB.182.23.6845-6849.2000.
[57] Partridge JD, Poole RK, Green J. The Escherichia coli *yhjA* gene, encoding a predicted cytochrome c peroxidase, is regulated by FNR and OxyR. Microbiology 2007;153:1499–509. https://doi.org/10.1099/mic.0.2006/004838-0.
[58] Zhao H, Zhang R, Yan X, Fan K. Superoxide dismutase nanozymes: an emerging star for anti-oxidation. J Mater Chem B 2021;9:6939–57. https://doi.org/10.1039/d1tb00720c.
[59] Lu J, Holmgren A. The thioredoxin antioxidant system. Free Radic Biol Med 2014;66:75–87. https://doi.org/10.1016/j.freeradbiomed.2013.07.036.
[60] Hicks JL, Mullholland CV. Cysteine biosynthesis in *Neisseria* species. Microbiology 2018;164:1471–80. https://doi.org/10.1099/mic.0.000728.
[61] Kalnenieks U, Balodite E, Rutkis R. Metabolic engineering of bacterial respiration: high vs. low P/O and the case of *Zymomonas mobilis*. Front Bioeng Biotechnol 2019;7:327. https://doi.org/10.3389/fbioe.2019.00327.
[62] Imlay JA. The molecular mechanisms and physiological consequences of oxidative stress: lessons from a model bacterium. Nat Rev Microbiol 2013;11:443–54. https://doi.org/10.1038/nrmicro3032.
[63] Souza LL, Eduardo IR, Padula M, Leitao AC. Endonuclease IV and exonuclease III are involved in the repair and mutagenesis of DNA lesions induced by UVB in *Escherichia coli*. Mutagenesis 2006;21:125–30. https://doi.org/10.1093/mutage/gel006.
[64] Abula A, Yang T, Zhang Y, Li T, Ji X. Enhancement of *Escherichia coli* ribonuclease R cytosine-sensitive activity by single amino acid substitution. Mol Biotechnol 2022;65:108–15. https://doi.org/10.1007/s12033-022-00533-w.
[65] Schormann N, Ricciardi R, Chattopadhyay D. Uracil-DNA glycosylases-structural and functional perspectives on an essential family of DNA repair enzymes. Protein Sci 2014;23:1667–85. https://doi.org/10.1002/pro.2554.
[66] Park N, Heo J, Song S, Jo I, Lee K, Ha N-C. Crystal structure of *Streptomyces coelicolor* RraAS2, an unusual member of the RNase E inhibitor RraA protein family. J Microbiol 2017;55:388–95. https://doi.org/10.1007/s12275-017-7053-8.
[67] Feliciello I, Ljubić S, Đermić E, Ivanković S, Zahradka D, Đermić D. Single-strand DNA-binding protein suppresses illegitimate recombination in *Escherichia coli*, acting in synergy with RecQ helicase. Sci Rep 2024;14:20476. https://doi.org/10.1038/s41598-024-70817-5.
[68] Ruan B, Söll D. The bacterial YbaK protein is a Cys-tRNA^{Pro} and Cys-tRNA^{Cys} deacylase. J Biol Chem 2005;280:25887–91. https://doi.org/10.1074/jbc.M502174200.
[69] Djaman O, Outten FW, Imlay JA. Repair of oxidized iron-sulfur clusters in *Escherichia coli*. J Biol Chem 2004;279:44590–9. https://doi.org/10.1074/jbc.M406487200.
[70] Sen A, Imlay JA. How microbes defend themselves from incoming hydrogen peroxide. Front Immunol 2021;12:667343. https://doi.org/10.3389/fimmu.2021.667343.
[71] Wan F, Yin J, Sun W, Gao H. Oxidized OxyR Up-Regulates ahpCF expression to suppress plating defects of oxyR- and catalase-deficient strains. Front Microbiol 2019;10:439. https://doi.org/10.3389/fmicb.2019.00439.
[72] Seo Sang W, Kim D, Szubin R, Palsson Bernhard O. Genome-wide reconstruction of OxyR and SoxRS transcriptional regulatory networks under oxidative stress in *Escherichia coli* K-12 MG1655. Cell Rep 2015;12:1289–99. https://doi.org/10.1016/j.celrep.2015.07.043.
[73] Imlay JA. Cellular defenses against superoxide and hydrogen peroxide. Annu Rev Biochem 2008;77:755–76. https://doi.org/10.1146/annurev.biochem.77.061606.161055.
[74] Jang S, Imlay JA. Hydrogen peroxide inactivates the *Escherichia coli* Isc iron-sulphur assembly system, and OxyR induces the Suf system to compensate. Mol Microbiol 2010;78:1448–67. https://doi.org/10.1111/j.1365-2958.2010.07418.x.
[75] Hu W, Li W, Chen J. Recent advances of microbial breeding via heavy-ion mutagenesis at IMP. Lett Appl Microbiol 2017;65:274–80. https://doi.org/10.1111/lam.12780.
[76] Zhang X, Zhang XF, Li HP, Wang LY, Zhang C, Xing XH, Bao CY. Atmospheric and room temperature plasma (ARTP) as a new powerful mutagenesis tool. Appl Microbiol Biotechnol 2014;98:5387–96. https://doi.org/10.1007/s00253-014-5755-y.
[77] Cooke MS, Evans MD, Dizdaroglu M, Lunec J. Oxidative DNA damage: mechanisms, mutation, and disease. FASEB J 2003;17:1195–214. https://doi.org/10.1096/fj.02-0752rev.
[78] Gaunt LF, Beggs CB, Georghiou GE. Bactericidal action of the reactive species produced by gas-discharge nonthermal plasma at atmospheric pressure: a review. IEEE Trans Plasma Sci 2006;34:1257–69. https://doi.org/10.1109/tps.2006.878381.
[79] Matsumoto KI, Ueno M, Shoji Y, Nakanishi I. Heavy-ion beam-induced reactive oxygen species and redox reactions. Free Radic Res 2021;55:450–60. https://doi.org/10.1080/10715762.2021.1899171.
[80] Choi H-J, Kim S-J, Mukhopadhyay P, Cho S, Woo J-R, Storz G, Ryu S-E. Structural basis of the redox switch in the OxyR transcription factor. Cell 2001;105:103–13. https://doi.org/10.1016/s0092-8674(01)00300-2.
[81] Su L, Li S, Li X, Wang F, Lin L, Lin Y. Enhancing oxidative tolerance and fermentation performance of *Lactobacillus casei* through adaptive laboratory evolution. LWT 2025;224. https://doi.org/10.1016/j.lwt.2025.117826.
[82] Lu M, Sha Y, Kumar V, Xu Z, Zhai R, Jin M. Transcription factor-based biosensor: a molecular-guided approach for advanced biofuel synthesis. Biotechnol Adv 2024;72. https://doi.org/10.1016/j.biotechadv.2024.108339.
[83] Ding N, Zhou S, Deng Y. Transcription-factor-based biosensor engineering for applications in synthetic biology. ACS Synth Biol 2021;10:911–22. https://doi.org/10.1021/acssynbio.0c00252.
[84] Zheng M, Wang X, Templeton LJ, Smulski DR, LaRossa RA, Storz G. DNA microarray-mediated transcriptional profiling of the *Escherichia coli* response to hydrogen peroxide. J Bacteriol 2001;183:4562–70. https://doi.org/10.1128/jb.183.15.4562-4570.2001.
[85] Altuvia S, Weinstein-Fischer D, Zhang A, Postow L, Storz G. A small, stable RNA induced by oxidative stress: role as a pleiotropic regulator and antimutator. Cell 1997;90:43–53. https://doi.org/10.1016/s0092-8674(00)80312-8.
[86] Roop RM, Phillips PL, Reyes L, Sampson EM, Murrell EA, Whitlock JA, Progulske-Fox A. Deletion of a conserved transcript PG_RS02100 expressed during logarithmic growth in *Porphyromonas gingivalis* results in hyperpigmentation and increased tolerance to oxidative stress. PLoS One 2018;13. https://doi.org/10.1371/journal.pone.0207295.
[87] Gupta A, Imlay JA. Escherichia coli induces DNA repair enzymes to protect itself from low-grade hydrogen peroxide stress. Mol Microbiol 2022;117:754–69. https://doi.org/10.1111/mmi.14870.
[88] Utrilla J, O'Brien Edward J, Chen K, McCloskey D, Cheung J, Wang H, Armenta-Medina D, Feist Adam M, Palsson Bernhard O. Global rebalancing of cellular

resources by pleiotropic point mutations lllustrates a multi-scale mechanism of adaptive evolution. Cell Syst 2016;2:260–71. https://doi.org/10.1016/j.cels.2016.04.003.

[89] Suski JM, Lebiedzinska M, Bonora M, Pinton P, Duszynski J, Wieckowski MR. Relation between mitochondrial membrane potential and ROS formation. In: Palmeira CM, Oliveira PJ, editors. Mitochondrial Bioenergetics. Methods in Molecular Biology. New York, NY: Humana; 2012. p. 183–205.

[90] Zhu Z, Ding X, Rang J, Xia L. Application and research progress of ARTP mutagenesis in actinomycetes breeding. Gene 2024;929. https://doi.org/10.1016/j.gene.2024.148837.

[91] Zeng R, Xu J, Liang T, Li M, Tang D. Photocurrent-Polarity-Switching Photoelectrochemical biosensor for switching spatial distance electroactive tags. ACS Sens 2023;8:317–25. https://doi.org/10.1021/acssensors.2c02314.

[92] Huang L, Cai G, Zeng R, Yu Z, Tang D. Contactless photoelectrochemical biosensor based on the ultraviolet-assisted gas sensing interface of three-dimensional SnS(2) nanosheets: from mechanism reveal to practical application. Anal Chem 2022;94:9487–95. https://doi.org/10.1021/acs.analchem.2c02010.